Acta Mech 229, 3143–3160 (2018)
https://doi.org/10.1007/s00707-018-2179-2

ORIGINAL PAPER

Wuyi Wan · **Wenrui Huang**

Water hammer simulation of a series pipe system using the MacCormack time marching scheme

Received: 10 January 2018 / Revised: 30 March 2018 / Published online: 31 May 2018

Abstract Transient simulation is very important to protect the water supply pipeline system from extreme pressures. In order to numerically simulate the transient response in a variable–property series pipe system, the water hammer model and matched boundary conditions are developed by introducing the MacCormack time marching scheme. Based on the proposed method, the transient pressure and flow velocity are numerically predicted for a variable–property series pipe, and then the results are compared to the classical method of characteristics (MOC). The improved method can yield a reasonable numerical solution for a closed pipe, and the solution agrees well with the MOC and existing experimental results. In the proposed model, the time step is no longer subjected to the length of the space step; consequently, it is more convenient in meshing and modifying the $x - t$ grid. Especially, it is very advantageous in establishing the simultaneous calculation in water hammer simulation for a variable–property series pipes system or complicated distribution networks.

List of symbols

A	Area of section (m^2)
a	Wave speed of water hammer (m/s)
C	Constant
Z_u	Upstream constant water level (m)
C^*	Vardy's shear decay coefficient
C_d	Discharge coefficient of valve
C_T	Dimensionless time consumed
C_R	Refining coefficient of time interval
C_{TMO}	Dimensionless time consumed in MOC
C_{TMT}	Dimensionless time consumed in MTMS
C_{TR}	The ratio of the computing times
C_x	Dimensionless space step
D	Main pipe diameter (m)

The project was supported by National Natural Science Foundation of China (Grant Nos. 51779216, 51279175) and Zhejiang Provincial Natural Science Foundation of China (Grant No. LZ16E090001).

W. Wan (✉)
Department of Hydraulic Engineering, College of Civil Engineering and Architecture, Zhejiang University, Hangzhou 310058, People's Republic of China
E-mail: wanwuyi@zju.edu.cn

W. Huang
Department of Civil and Environmental Engineering, Florida State University, Tallahassee, FL 32310, USA
E-mail: whuang@fsu.edu

e	Internal energy (J)
f	Darcy–Weisbach friction factor
f_{q}	Quasi-steady friction factor
g	Acceleration of gravity (m/s^2)
h	Pressure head (m)
h_{ns}	The head of the valve (m)
h_w	The head loss between section (m)
i	Serial number of nodes (s)
j	Serial number of nodes (s)
k	Brunone friction coefficient
n	The number of elements in a single pipe
p_{a}	Atmospheric pressure (Pa)
p	Pressure (Pa)
Q	Instantaneous discharge at section (m^3/s)
s	Section area at nodes (m^2)
S	Square integral domain
$\mathbf{S}$	Vector surface area
T	Time (s)
t	Time, as subscript to denote time (s)
T_{MO}	Total time consumed in MOC
T_{MT}	Total time consumed in MTMS
v	Flow velocity (m/s)
$\mathbf{v}$	Velocity vector
x	Distance along pipe from the inlet (m)
θ	Pipe slope
ρ	Fluid density (kg/m^3)
Δx	Length of element, space interval step (m)
C_{xMO}	Dimensionless space step in MOC
C_{xMT}	Dimensionless space step in MTMS
Δt	Time interval step (s)
Ω	Volume integral domain

Symbols

$\sim$	Superscript denotes estimated values
$-$	Superscript denotes average values

Abbreviations

MOC	Method of characteristics
MTMS	MacCormack time marching scheme
FW	Forward wave
RW	Reverse wave

1 Introduction

Water hammer can cause severe vibrations, cavitations, and breaks in a pipes system [1]. It is very important to simulate and control the water hammer in pressurized-pipe system [2,3], in order to protect the pipe apparatus in a pumps system [4,5], unclear system [6], and hydropower station [7,8]. Experimental and numerical simulations can be used to predict hydraulic transient processes, especially extreme pressures. However, in an experiment it is very difficult to combine the state and space boundary conditions. Moreover, an experiment also costs much in terms of time and expense. With the development of computers and computing techniques, numerical simulation is more widely used to predict water hammer in scientific and engineering applications.

Over the past few decades, various numerical methods have been developed to simulate and control hydraulic transient processes [9]. The most common method employed is the explicit-format method of characteristics (MOC) [1], which has been widely used and improved in the applications of multi-pipe systems [10]. Other approaches include the implicit-format method of characteristics [11] and the finite element method [12]. Typically, Guinot et al. [13] investigated the finite-volume method (FVM) for water hammer simulation, and proposed first-order and second-order approximate Riemann solvers using the Godunov scheme. Wood et al. [14] proposed the interesting wave characteristic method (WCM) based on pressure wave propagations and the pipe wall resistances in a single sonic flow. Kim et al. [15] proposed an impulse response method to analyze the transient process of water distribution systems with surge protection devices, and he also improved the impedance matrix method for transient computation of large pipe networks [16]. Niroomandi et al. [17] proposed a time-splitting projection method for simulating water hammer in deformable pipes. Alamian et al. [18] developed a state space model for water hammer simulation in gas pipelines and networks. Hwang [19] proposed a characteristic particle method to simulate the water hammer in piping systems.

As the most popular numerical method, explicit MOC is widely and conventionally used in the water hammer simulation induced by valves [20,21], pumps [22,23], and air pockets [24]. The implicit method of characteristics (IMOC) can be applied to more complicated water hammers in some particular conditions [6,11]; however, the irregular $x - t$ mesh and complicated data structure have significantly limited its application. Moreover, some mixed-method coupled traditional MOC has also been proposed to simulate the water hammer [25]. As a second-order finite difference method, the MacCormack method [26] is widely used to solve the hyperbolic partial differential equation in computational fluid dynamics [27–30]. However, the method hardly plays its role in practical water hammer simulation and prediction. In fact, Chaudhry [12] referred briefly to the method for solving the water hammer equation in general middle nodes. Amara [31] applied the method to solve the middle node of water hammer in a single pipe. However, the literature has not considered the convective acceleration terms, and no matched end boundaries were established. Because the end boundaries still depend on the characteristic line method, the time and space step cannot be defined independently.

In this paper, the improved approach, including regular nodes and matched boundary model, is established to numerically simulate the water hammer in a subsonic-flow pipeline system. The MacCormack time marching scheme (MTMS) is used to simulate the water hammer in a variable–property series pipe system; especially, the convective acceleration terms and matched end boundaries were considered. The proposed method is generally different from the MOC in structure and boundary constraints. In this method, the numerical solution is first established using the MTMS, and the matched boundary conditions models are developed for the valve and connection in a variable–property pipe system. The time step is no longer subjected to the space interval step when meshing the $x - t$ grid. It can decrease the computing time by optimizing the computational grid. Moreover, for a variable–property series pipe system, the new method is convenient to select the same time step for all pipes without wave-speed adjustment or interpolation, since the time step is no longer depending on the space step. It is therefore more efficient in the numerical simulation of water hammer analysis for a variable–property pipe system.

2 Control equations of transient flow

2.1 Basic fluid dynamics equations

The general physical equation system of the fluid movement consists of the continuity equation, momentum equation, and energy equation. They can be expressed as a closed equation system as follows [28]:

$$\begin{bmatrix} \frac{\partial}{\partial t}\iiint_{\Omega}\rho \mathrm{d}\Omega + \iint_{S}\rho\mathbf{v}\cdot\mathrm{d}\mathbf{S} \\ \frac{\partial}{\partial t}\iiint_{\Omega}\rho\mathbf{v}\mathrm{d}\Omega + \iint_{S}\rho\mathbf{v}\,(\mathbf{v}\cdot\mathrm{d}\mathbf{S}) \\ \frac{\partial}{\partial t}\iiint_{\Omega}\rho\left(e+\frac{\mathbf{v}^2}{2}\right)\mathrm{d}\Omega + \iint_{S}\rho\left(e+\frac{\mathbf{v}^2}{2}\right)\mathbf{v}\cdot\mathrm{d}\mathbf{S} \end{bmatrix} = \begin{bmatrix} 0 \\ -\iint_{S}p\mathrm{d}\mathbf{S} + \frac{\partial}{\partial t}\iiint_{\Omega}\rho\mathbf{g}\mathrm{d}\Omega \\ -\iint_{S}p\mathbf{v}\cdot\mathrm{d}\mathbf{S} + \frac{\partial}{\partial t}\iiint_{\Omega}\rho\mathbf{g}\mathbf{v}\mathrm{d}\Omega \end{bmatrix}. \quad (1)$$

2.2 Control equations for closed-pipe flow

For the one-dimensional flow in a closed pipe, considered as an isothermal process, without energy transformation, the flow is only subjected to the continuity and momentum equations. Therefore, the system of equations

can be written as follows:

$$\begin{bmatrix} \frac{\partial(\rho A)}{\partial t} + \frac{\partial(\rho A v)}{\partial x} \\ \rho \frac{\partial v}{\partial t} + \rho v \frac{\partial v}{\partial x} \end{bmatrix} = \begin{bmatrix} 0 \\ -\frac{\partial p}{\partial x} \end{bmatrix}. \tag{2}$$

Considering the friction of the pipe wall, in the pressure head form, the general water hammer equations of a pipe flow can be expressed as [1]

$$\begin{bmatrix} \frac{\partial h}{\partial t} + v \frac{\partial h}{\partial x} + \frac{a^2}{g} \frac{\partial v}{\partial x} - v \sin\theta \\ \frac{\partial v}{\partial t} + g \frac{\partial h}{\partial x} + v \frac{\partial v}{\partial x} + \frac{f v|v|}{2D} \end{bmatrix} = \begin{bmatrix} 0 \\ 0 \end{bmatrix}. \tag{3}$$

Equation (3) combines the entire system of equations to describe the water hammer process in a closed-pipe system. Here, the general continuity and movement equations are briefly introduced, especially, because they are fundamental for water hammer simulation in a closed-pipe system. Similarly, they are also used in the following analysis. In general, while solving, the convective acceleration terms are commonly omitted to simplify the simultaneous equations in conventional methods [1,12,14,31]. This is reasonable when the wave speed is much more important than the pipe flow velocity. In fact, the waves propagate with the speed of $v + a$ in the forward direction and $v - a$ in the backward direction. For some elastic pipes, the influence of the flow velocity on the water simulation is significant, which requires extra interpolation and a more complex solving process.

The aim of this paper is to establish an entire solution model for the closed expressed equations by introducing the MTMS. Matched boundary condition constraints are analyzed and established for coupling the proposed model. In the proposed model, all terms will not be omitted in the derivation, and it still has the regular $x - t$ mesh structure and accurate solutions. Especially, the time step is no longer subjected to the characteristics line when meshing the $x - t$ grids.

3 Solution model of transient flow

3.1 Water hammer model in MTMS

3.1.1 Numerical discrete format for partial differential equation

The MacCormack method [26] has been used to solve hyperbolic partial differential equations in computational fluid dynamics [27–30]. It has also been used to solve water hammer equations without convective acceleration terms [12,31]. As seen, Eq. (3) consists of two hyperbolic partial differential equations. In order to establish a two-variable iterative model in MTMS, Eq. (3) can be written in the time marching format as

$$\begin{bmatrix} \frac{\partial h}{\partial t} \\ \frac{\partial v}{\partial t} \end{bmatrix} = \begin{bmatrix} -v \frac{\partial h}{\partial x} - \frac{a^2}{g} \frac{\partial v}{\partial x} + v \sin\theta \\ -g \frac{\partial h}{\partial x} - v \frac{\partial v}{\partial x} - \frac{f v|v|}{2D} \end{bmatrix}. \tag{4}$$

In Eq. (4), f is the general Darcy–Weisbach friction factor. In the classical MOC model, the coefficient is approximately treated as a quasi-steady friction factor f_q. Bergant et al. [32–34] clearly showed that the quasi-steady friction method can effectively simulate the peak pressure at the first and second pulse. However, in the simulation of rapid water hammer, there may be some deviations in the attenuation and phase shift of the pressure surges. In order to analyze the effects of unsteady friction, several typical models have been proposed by Zielke [35], Hino et al. [36], and Brunone et al. [37]. These models are widely applied and improved to evaluate the unsteady friction [32–34,38–44]. Especially, many studies show that the Brunone model is almost the most popular model and the form has been continuously improved [34,38,39]. The model takes into account the instantaneous local acceleration $\partial v/\partial t$ and the instantaneous convective acceleration $\partial v/\partial x$ on the unsteady head losses. Therefore, the model is also selected to evaluate the unsteady friction in the presented research. The latest form can be written as [38]

$$f = f_q + \frac{2kD}{v|v|} \left(\frac{\partial v}{\partial t} + \mathrm{sgn}(v) a \left| \frac{\partial v}{\partial x} \right| \right). \tag{5}$$

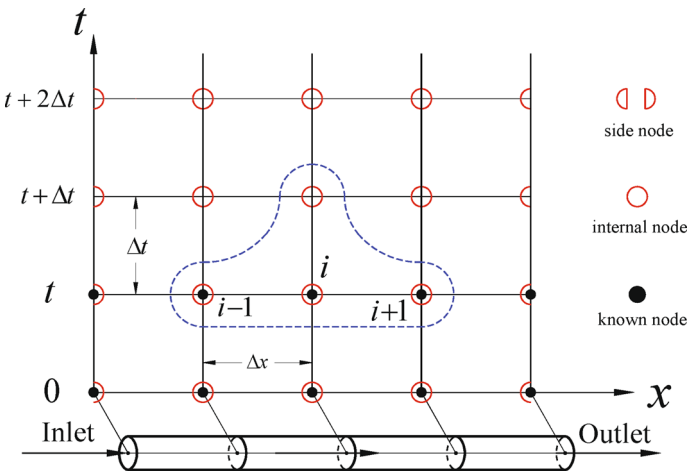

Fig. 1 Time marching mesh for a pipe flow

According to Vardy's shear decay coefficient C^*, the Brunone friction coefficient is calculated empirically [34,45],

$$k = \frac{\sqrt{C^*}}{2} \begin{cases} C^* = 0.00476 & \text{For laminar flow} \\ C^* = 7.41/\mathrm{Re}^{\log(14.3/\mathrm{Re}^{0.05})} & \text{For turbulent flow.} \end{cases} \tag{6}$$

Therefore, Eq. (4) can be converted into the following form:

$$\begin{bmatrix} \frac{\partial h}{\partial t} \\ \frac{\partial v}{\partial t} \end{bmatrix} = \begin{bmatrix} -v\frac{\partial h}{\partial x} - \frac{a^2}{g}\frac{\partial v}{\partial x} + v\sin\theta \\ \left(-g\frac{\partial h}{\partial x} - v\frac{\partial v}{\partial x} - \mathrm{sign}(v)ka\left|\frac{\partial v}{\partial x}\right| - \frac{f_q v|v|}{2D}\right)(1+k)^{-1} \end{bmatrix}. \tag{7}$$

To express the discretization scheme and solve the marching process clearly, next, a simple time marching mesh is illustrated. Figure 1 shows an $x - t$ grid for a single closed pipe, which is meshed over five sections (nodes), and the time interval Δt is specified as the marching time step. Especially, the time step is no longer subjected to the space step (length of the element) depending on the characteristics path line. Consequently, without the limitation of the characteristics line, it is convenient to modify the time step and space step in order to optimize the computational mesh. Three kinds of nodes are marked in Fig. 1. The solid dot, denoting the node, is known at the beginning of the present time step. The entire hollow circle denotes the unknown internal nodes, which have two adjacent nodes. The semicircle denotes the unknown side nodes, which have only an adjacent node in the left or right.

In the figure, the marching step is always from the known nodes to the unknown nodes. According to the known nodes, in the forward difference format, the general spatial derivatives of node i at the beginning of the present step can be written as

$$\begin{bmatrix} \left(\frac{\partial h}{\partial t}\right)_i^t \\ \left(\frac{\partial v}{\partial t}\right)_i^t \end{bmatrix} = \begin{bmatrix} -v_i^t\frac{h_{i+1}^t - h_i^t}{\Delta x} - \frac{a^2}{g}\frac{v_{i+1}^t - v_i^t}{\Delta x} + v_i^t\sin\theta \\ \left(-g\frac{h_{i+1}^t - h_i^t}{\Delta x} - v_i^t\frac{v_{i+1}^t - v_i^t}{\Delta x} - \mathrm{sgn}(v_i^t)ka\left|\frac{v_{i+1}^t - v_i^t}{\Delta x}\right| - \frac{f_q v_i^t|v_i^t|}{2D}\right)(1+k)^{-1} \end{bmatrix}. \tag{8}$$

According to the spatial derivatives, the value of node i at time $t + \Delta t$ can be estimated as

$$\begin{bmatrix} \tilde{h}_i^{t+\Delta t} \\ \tilde{v}_i^{t+\Delta t} \end{bmatrix} = \begin{bmatrix} h_i^t + \left(-v_i^t\frac{h_{i+1}^t - h_i^t}{\Delta x} - \frac{a^2}{g}\frac{v_{i+1}^t - v_i^t}{\Delta x} + v_i^t\sin\theta\right)\Delta t \\ v_i^t - \left\{-g\frac{h_{i+1}^t - h_i^t}{\Delta x} - v_i^t\frac{v_{i+1}^t - v_i^t}{\Delta x} - \mathrm{sgn}(v_i^t)ka\left|\frac{v_{i+1}^t - v_i^t}{\Delta x}\right| - \frac{f_q v_i^t|v_i^t|}{2D}\right\}(1+k)^{-1}\Delta t \end{bmatrix}. \tag{9}$$

Similarly, the value of node $i-1$ at time $t+\Delta t$ can be estimated as

$$\begin{bmatrix} \tilde{h}_{i-1}^{t+\Delta t} \\ \tilde{v}_{i-1}^{t+\Delta t} \end{bmatrix} = \begin{bmatrix} h_{i-1}^{t} + \left(-v_{i-1}^{t} \frac{h_i^t - h_{i-1}^t}{\Delta x} - \frac{a^2}{g} \frac{v_i^t - v_{i-1}^t}{\Delta x} + v_{i-1}^t \sin\theta \right) \Delta t \\ v_{i-1}^{t} - \left(-g \frac{h_i^t - h_{i-1}^t}{\Delta x} - v_{i-1}^t \frac{v_i^t - v_{i-1}^t}{\Delta x} - k \mathrm{sgn}(v_{i-1}^t) a \left| \frac{v_i^t - v_{i-1}^t}{\Delta x} \right| - \frac{f_q v_{i-1}^t |v_{i-1}^t|}{2D} \right) (1+k)^{-1} \Delta t \end{bmatrix}. \tag{10}$$

Based on the estimated value at time $t+\Delta t$, in rearward differences, the spatial derivatives of node i at time $t+\Delta t$ can be estimated as

$$\begin{bmatrix} \left(\frac{\partial h}{\partial t}\right)_i^{t+\Delta t} \\ \left(\frac{\partial v}{\partial t}\right)_i^{t+\Delta t} \end{bmatrix} = \begin{bmatrix} -\tilde{v}_i^{t+\Delta t} \frac{\tilde{h}_i^{t+\Delta t} - \tilde{h}_{i-1}^{t+\Delta t}}{\Delta x} - \frac{a^2}{g} \frac{\tilde{v}_i^{t+\Delta t} - \tilde{v}_{i-1}^{t+\Delta t}}{\Delta x} + \tilde{v}_i^{t+\Delta t} \sin\theta \\ \left(-g \frac{\tilde{h}_i^{t+\Delta t} - \tilde{h}_{i-1}^{t+\Delta t}}{\Delta x} - \tilde{v}_i^{t+\Delta t} \frac{\tilde{v}_i^{t+\Delta t} - \tilde{v}_{i-1}^{t+\Delta t}}{\Delta x} - \mathrm{sgn}(\tilde{v}_i^{t+\Delta t}) k a \left| \frac{\tilde{v}_i^{t+\Delta t} - \tilde{v}_{i-1}^{t+\Delta t}}{\Delta x} \right| - \frac{f_q \tilde{v}_i^{t+\Delta t} \left| \tilde{v}_i^{t+\Delta t} \right|}{2D} \right) (1+k)^{-1} \end{bmatrix}. \tag{11}$$

3.1.2 Solution model for regular nodes

Equation (9) estimates the value of node i at time $t+\Delta t$ using the spatial derivatives of node i at time t. As a correction, the spatial derivative can be replaced by the average at the present step, which can be calculated by combining Eqs. (8) and (11) as follows:

$$\begin{bmatrix} \left(\overline{\frac{\partial h}{\partial t}}\right)_i^{t+\Delta t/2} \\ \left(\overline{\frac{\partial v}{\partial t}}\right)_i^{t+\Delta t/2} \end{bmatrix} = \frac{1}{2} \begin{bmatrix} \left(\frac{\partial h}{\partial t}\right)_i^{t} + \left(\frac{\partial h}{\partial t}\right)_i^{t+\Delta t} \\ \left(\frac{\partial v}{\partial t}\right)_i^{t} + \left(\frac{\partial v}{\partial t}\right)_i^{t+\Delta t} \end{bmatrix}. \tag{12}$$

Thus, the corrected value of node i at time $t+\Delta t$ can be obtained by Eq. (13). The final solution can be written as

$$\left[\begin{matrix} h_i \\ v_i \end{matrix} \right] \Bigg| \, t+\Delta t = \left[\begin{matrix} h_i \\ v_i \end{matrix} \right] \Bigg|_{\, t} + \Delta t \left[\left(\overline{\frac{\partial h}{\partial t}}\right)_i^{t+\Delta t/2} \left(\overline{\frac{\partial v}{\partial t}}\right)_i^{t+\Delta t/2} \right]^{\mathrm{T}}. \tag{13}$$

The model can yield all values at time $t+\Delta t$ for all internal nodes, as shown in Fig. 1. Unlike the conventional water hammer simulation, as seen in the derivation process, the proposed model still includes the convective acceleration terms. The wave propagations are separately considered with different speeds in the forward and backward directions, and the regular, fixed $x-t$ mesh is still available in the proposed model. Theoretically, it is very convenient and most suited for all water hammer simulations in a closed-pipe system.

In MOC, the wave propagates with the same speed in both forward and backward directions, so a regular fixed $x-t$ mesh can be established, which is very convenient in practical application. In theory, a slight deviation in phase shift may raise, since the effect of the flow velocity is neglected. IMOC is suitable for an elastic pipe, but the irregular $x-t$ grids limit its application. WCM can simplify the calculation and save time, but it cannot give the extreme pressure along the pipe. MTMS is improved to make up for these deficiencies. (i) The new method includes the convective acceleration term, which considers separately the different wave speeds in the forward and backward directions, so it is also suitable for application to elastic pipes. (ii) The method still uses a regular $x-t$ grid, so it is elegant and convenient to apply. (iii) It can provide the extreme pressure along the pipeline, so it is easy to predict the weakest section due to the internal transient pressure.

3.2 General boundary model for single subsonic pipe flow

As shown in Fig. 2, a single pipe commonly includes only an inlet boundary and an outlet boundary. For subsonic flow, the forward wave speed $v+a$ is always larger than zero, and the reverse wave speed $v-a$ is always less than zero. Consequently, in the inlet, the forward wave (FW) always propagates into the pipe flow domain, and the rearward wave (RW) always propagates out the pipe flow domain. Conversely, in the outlet, the FW always propagates out the pipe flow domain, and the RW propagates into the pipe flow domain. If the inlet and outlet are free, the boundary condition can be written as [28]

$$h_i^{t+\Delta t} = 2h_{i+1}^{t+\Delta t} - h_{i+2}^{t+\Delta t} \tag{14}$$

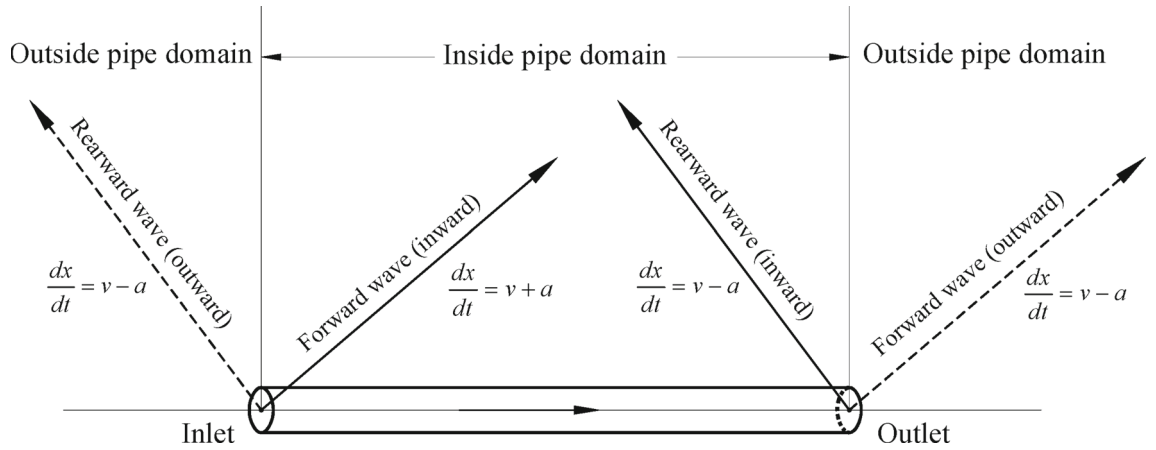

Fig. 2 Boundary conditions for a single isotropic pipe

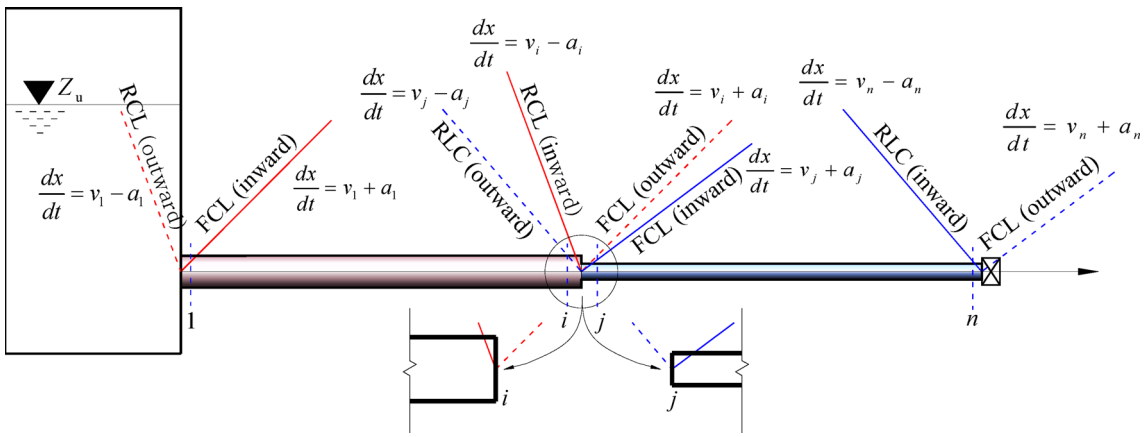

Fig. 3 Boundary conditions for a series variable pipe system

or

$$v_i^{t+\Delta t} = 2v_{i+1}^{t+\Delta t} - v_{i+2}^{t+\Delta t}. \tag{15}$$

3.3 Boundary model for variable–property pipes in series

In fact, the two sides of the single pipe are always restrained by connecting to other pipes and devices in a closed-pipe system. The boundary conditions vary with the connection type. Figure 3 illustrates the basic components and the boundary conditions of a variable–property series pipe system. The system consists of the upstream pool with a steady water level, the junction connecting two variable–property pipes, and the control valve at the end. These boundary models needed in the system are very useful and convenient in the water hammer simulation.

3.3.1 Inlet boundary condition

In the inlet, the forward wave (FW) propagates into the pipe flow domain, and the rearward wave (RW) propagates out of the pipe flow domain. Thus, the boundary condition includes an independent variable and a dependent variable. For a constant upstream water level, the boundary constraint condition can be written as

$$\left\{ h_1^{t+\Delta t} = Z_{\mathrm{u}},\ \frac{\partial h_1}{\partial t} = 0 \right\}. \tag{16}$$

The final solution can be established as

$$\begin{bmatrix} h_1^{t+\Delta t} \\ v_1^{t+\Delta t} \end{bmatrix} = \begin{bmatrix} Z_{\mathrm{u}} \\ -a^2 v_2^{t+\Delta t} / \left[\left(h_2^{t+\Delta t} - h_1^{t+\Delta t} - \Delta x \sin\theta \right) g - a^2 \right] \end{bmatrix}. \tag{17}$$

3.3.2 Connection section boundary

In the connection section, both sides have a characteristic line that enters into the pipe flow domain. According to the continuity condition and head condition, the boundary constraint conditions can be expressed as

$$\left\{ \begin{array}{c} h_i^{t+\Delta t} = h_j^{t+\Delta t}, \partial h_i / \partial t = \partial h_j / \partial t \\ s_i v_i^{t+\Delta t} = s_j v_j^{t+\Delta t}, s_i \partial v_i / \partial t = s_j \partial v_j / \partial t \end{array} \right\}. \tag{18}$$

The solution of the equations can be written as

$$\begin{bmatrix} h_i^{t+\Delta t} & v_i^{t+\Delta t} \\ h_j^{t+\Delta t} & v_j^{t+\Delta t} \end{bmatrix} = \begin{bmatrix} 1 & 1 \\ 1 & 1 \end{bmatrix} \begin{bmatrix} \left(h_{i-1}^{t+\Delta t} \Delta x_j + h_{j+1}^{t+\Delta t} \Delta x_i \right) / \left(\Delta x_i + \Delta x_j \right) & 0 \\ 0 & \left(v_{i-1}^{t+\Delta t} s_i \Delta x_j + v_{j+1}^{t+\Delta t} s_j \Delta x_i \right) / \left(s_i \Delta x_j + s_j \Delta x_i \right) \end{bmatrix}. \tag{19}$$

Especially, though $h_{i-1}^{t+\Delta t}$, $h_{j+1}^{t+\Delta t}$, $v_{i-1}^{t+\Delta t}$, and $v_{j+1}^{t+\Delta t}$ are the parameters at the end of the time step, they have been determined previously by the middle node model, as seen in Eq. (13).

3.3.3 Valve boundary control equation

A valve can induce water hammer in pipe systems. In general, the boundary model of the valve consists of compound simultaneous equations, which may yield an extraneous solution during the solution process in the quadratic equations system [1]. Especially, for the valve with a backflow, a check process is necessary to meet the valve resistance [23]. For subsonic pipe flow, the rearward characteristic line will propagate into the internal domain; thus, a variable needs to be specified. According to the additional constraint equation of the valve, choosing the head as the free variable, the solution model of the outlet can be written as

$$\left. \begin{bmatrix} h_{ns}^{t+\Delta t} \\ v_{ns}^{t+\Delta t} \end{bmatrix} = \begin{bmatrix} h_{ns} \\ \mathrm{sgn}\left(h_{ns} - p_a\right) C_d sqrt\left(2g \left| h_{ns} - p_a \right|\right) \end{bmatrix} \right| h_{ns} = 2h_{ns-1}^{t+\Delta t} - h_{ns-2}^{t+\Delta t}. \tag{20}$$

The flow rate at the end is zero after the valve is completely closed. Therefore, the velocity becomes known, and the boundary can be written as follows:

$$\left\{ v_{ns}^{t+\Delta t} = 0, \frac{\partial v_{ns}}{\partial t} = 0 \right\}. \tag{21}$$

Using backward difference, the solution model can be established as

$$\begin{bmatrix} h_{ns}^{t+\Delta t} \\ v_{ns}^{t+\Delta t} \end{bmatrix} = \begin{bmatrix} h_{ns}^{t} + a^2 v_{ns-1}^{t+\Delta t} / (g \Delta x) \\ 0 \end{bmatrix}. \tag{22}$$

Compared to the traditional valve boundary condition model, the valve boundary model is advantageous. The flow can be directly determined after the pressure is estimated by a simple extrapolation method. In the solution process, there is no extraneous solution, and the check step is avoided.

3.4 Initial state conditions

The initial value is very important to improve the calculations. They can be simulated by an iterative process from some specified values in computational fluid dynamics. For some complicated system, they can also be computed by unsteady flow simulation. Here, the initial boundary condition can be determined by solution at steady conditions. According to the head loss principle, the initial values of the nodes can be expressed as follows:

$$\left[\begin{array}{ll} v_i = v_0 A_0 / A_i & i = 1, 2 \ldots n \\ h_{i+1} = h_i - h_w^{i,j+1}\Big|_{h_1 = h_0} & i = 1, 2 \ldots n \end{array}\right]\Bigg|_{t=0}. \tag{23}$$

Equations (17), (19), and (20) establish the entire boundary numerical solution for the inlet, the connection, and the outlet in water hammer simulation. It is very important to obtain a reasonable solution in a closed-pipe unsteady flow. Equation (23) provides the initial values of the steady flow at the initial time. It makes sure that the initial parameters are reasonable and leads to a faster numerical convergence. Now, the regular middle nodes model and the boundary model, as well as the initial values, constitute simultaneously a self-governed water hammer numerical simulation system.

4 Model validation

4.1 Comparison with existing experiment for a single pipe

In order to validate the proposed model, the numerical simulation results are compared with the existing experimental measurement. In particular, the experiment was conducted by Bergant and Simpson et al. [32–34]. Here, it is simply introduced and referenced to verify the numerical simulation by the proposed model. The experimental apparatus consists of a single copper pipe with 37.2 m in length, 22 mm in internal diameter and a 1.63 mm in wall thickness and two pressurized tanks. The steady state flow velocity is 0.3 m/s, the upstream pressurized is 32.0 m, valve closure time is 0.09 s, wave speed is 1319 m/s, and the quasi-steady friction coefficient is 0.034. The details can be referred to the references [32–34]. With the same boundary conditions, three different models were used to simulate the instantaneous transient by fast valve closure in a single pipe. These compared models are separately the classical MOC, MTMS with steady friction, and MTMS with unsteady friction.

Figure 4 compares the transient pressure surges at the endpoint near the valve, and Fig. 5 compares the transient pressure surges at the midpoint of the pipe. As seen in Figs. 4 and 5, the MOC can accurately simulate the maximum pressure and the initial phases. However, the deviation occurs and increases with time during the last period. For MTMS with steady friction, it can obtain similar results with MOC. Obviously, the result of MTMS with unsteady friction is more consistent with the measurement, and this proposed method significantly reduces the deviation of attenuation and phase shifts.

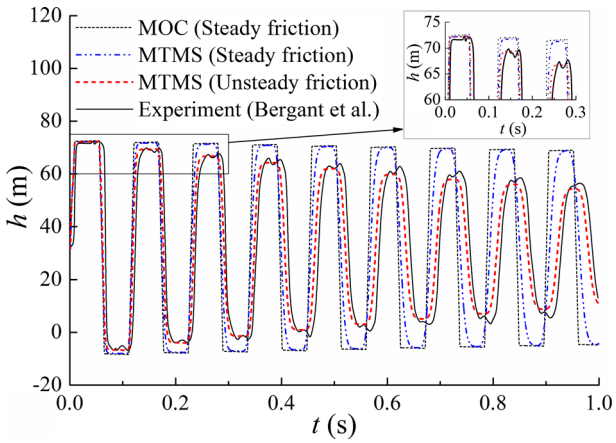

Fig. 4 Comparison of the transient pressure surges of the endpoint

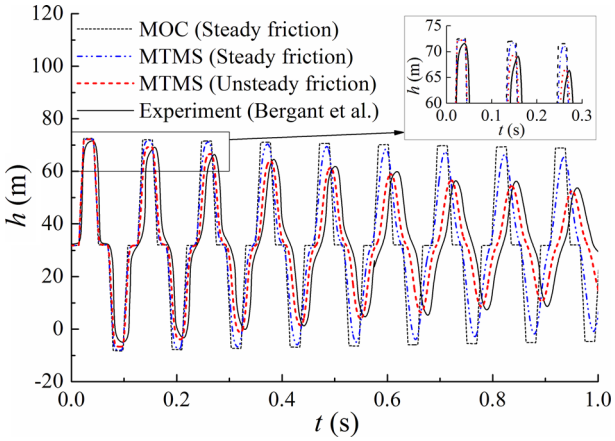

Fig. 5 Comparison of the transient pressure surges at the midpoint

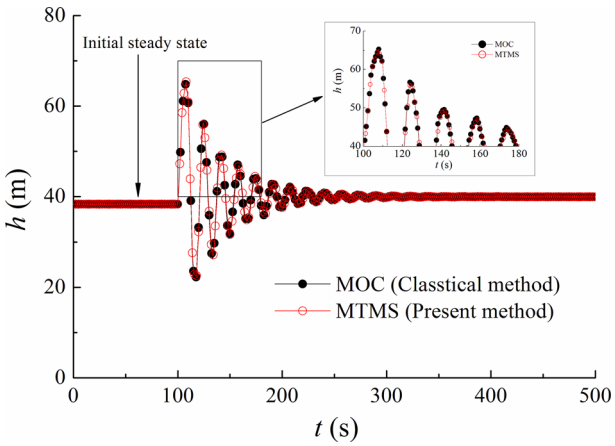

Fig. 6 Comparison of transient pressure process caused by valve closing

4.2 Variable–property pipes in series

In order to validate the proposed simulation method and boundary conditions model, a water hammer process is analyzed and simulated with MTMS and MOC. As shown in Fig. 3, the system consists of two different steel pipes in series and two reservoirs. The first pipe is 2720 m in length and 0.5 m in internal diameter, and the wave speed is 1000 m/s. The second pipe is 2652 m in length and 0.4 m in internal diameter, and the wave speed is 1200 m/s. The upstream water level is 40 m, and the flow discharge is 0.05 m^3/s. In order to generate a slow water hammer in the pipe system, the valve is partly closed in linear, and the flow changes from 0.05 to 0.01 m^3/s in 8 s. The pressure and flow fluctuation are analyzed and compared with the MOC method.

4.2.1 Transient pressure and flow process at a specific section

It is very important to predict the transient pressure and discharge processes in water hammer simulation. Based on the proposed method, Figs. 6 and 7 show the transient pressure head and flow, respectively, caused by closing the valve. In order to validate the result, simultaneously, the figure also shows the results solved by the traditional MOC method. As a traditional method, MOC has been verified and widely used to simulate water hammer in many research and industrial areas. By comparing the hydraulic process, the proposed method is verified to simulate the transient pressure and flow fluctuation in the connection section. Like MOC, it can also yield the same accurate numerical solution for water hammer in a closed pipe, including transient pressure and the flow process.

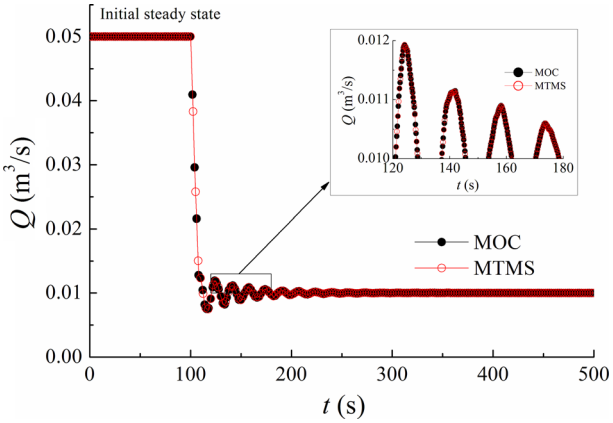

Fig. 7 Comparison of flow surge process caused by valve closing

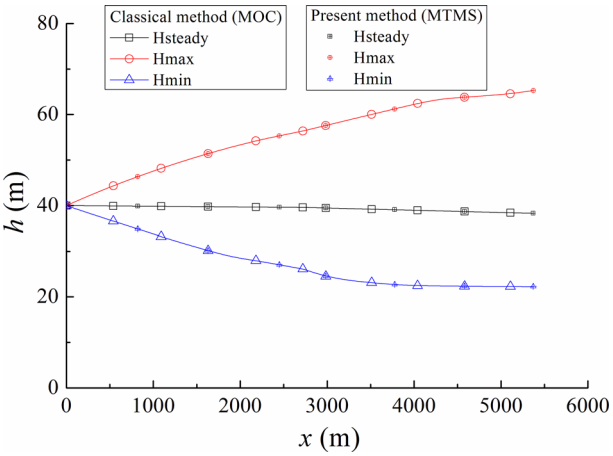

Fig. 8 Extreme transient pressure distribution along the pipeline

4.2.2 Extreme pressure distribution along the pipeline

Besides the end nodes, MTMS can compute all the internal nodes along the pipe. Consequently, the proposed method can provide the extreme pressure distribution along the pipe, which is important to determine the maximum internal pressure along the pipeline. Figure 8 shows the maximum and minimum pressure distribution along the entire pipeline. Analogously, MOC is also used to provide a reference to validate the new method. As shown in Fig. 6, both MTMS and MOC provide almost similar solutions with the same numerical precision. The comparison shows that the new method is capable of simulating the extreme pressure along the pipeline.

4.2.3 A fast water hammer analysis

As shown in the single pipe, the proposed method can improve the numerical results in attenuation and phase shifts. In order to analyze the rapid water hammer in the variable–property pipes in series, the same valve closure is completed in only 0.1 s. Figure 9 shows the transient pressure process of fast valve closure. As shown in Fig. 9, the result of the proposed model is similar to that of the classical model. In the enlarged figure, the slight deviation in attenuation and phase shifts comes out, since the instantaneous local acceleration and the instantaneous convective acceleration are taken into account. Unlike the complete valve closure, the unsteady friction has only slight effect on the transient process in a partial valve closure.

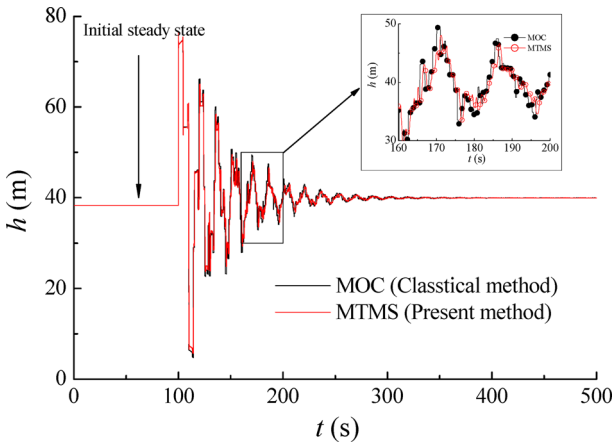

Fig. 9 Comparison of transient pressure process of fast valve closure

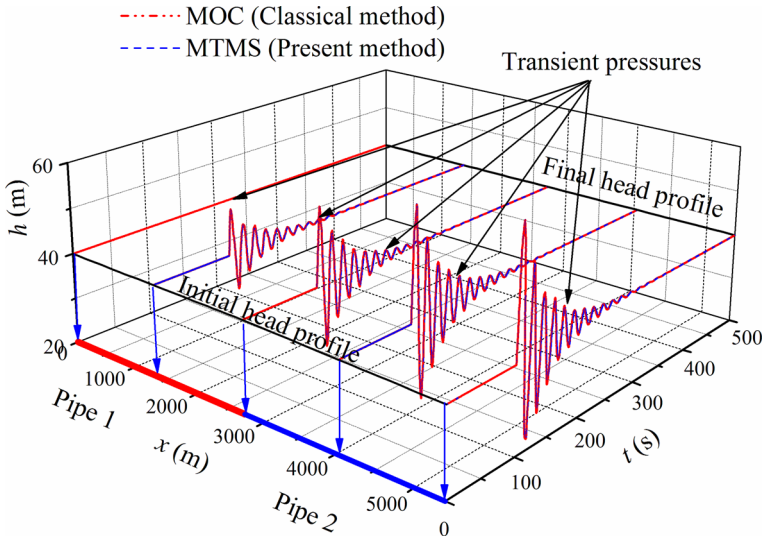

Fig. 10 Transient pressure process of various points along the pipe

4.3 Pressure and flow fluctuation at the pipeline

In Sect. 4.2, we compared the numerical results in the connection and extreme pressure along the pipe. Next, take the 8 s valve closure as an example, and all the pressure and flow fluctuations are simulated by the proposed MTMS. Figure 10 shows the transient pressure fluctuation process for the end and middle nodes along the pipeline. For each point, there are two lines: the red lines are the pressure processes simulated by MOC, and the blue lines are the pressure processes simulated by MTMS. As shown in Fig. 10, these results are almost overlapping, thus validating the proposed model. Analogously, Fig. 11 shows the transient flow processes in different sections. These results show that the proposed method can accurately simulate the transient process as with MOC.

4.4 Meshing constraint and time consumption analysis

4.4.1 Constraint on x–t meshing

In the fixed, explicit MOC format, in order to establish the fixed mesh, the time step is subjected to the distance step according to the characteristics path line. The constraint conditions of MOC can be expressed as

$$\Delta x = a\Delta t. \tag{24}$$

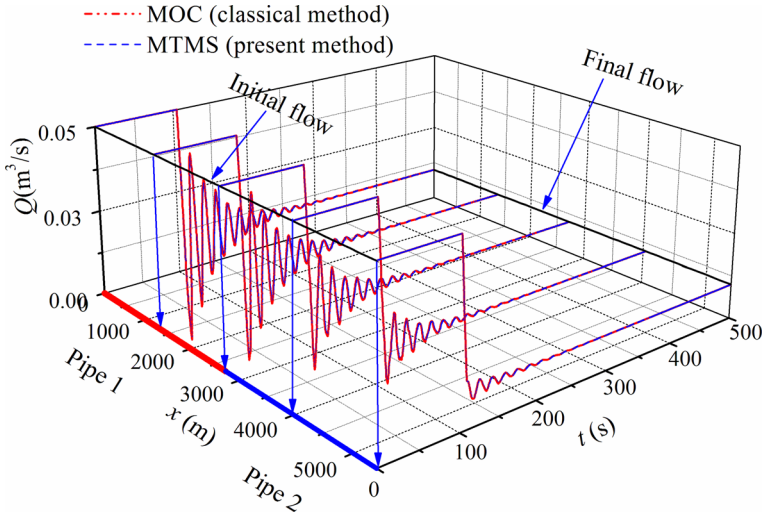

Fig. 11 Transient flow process of various points along the pipe

The constraint conditions of MTMS can be expressed as Courant condition [28]

$$\Delta x \geq (a + |v|)\,\Delta t. \tag{25}$$

Compared to the traditional method, MTMS is not constrained by the characteristic line. In MOC format, the space step increment and the time increment are strictly one to one correspondence. In other words, every space step increment is fixed with a given time step increment. However, in the proposed method, the time step and the space step can more freely be chosen within the Courant condition. As shown in Fig. 1, the $x - t$ grid is still regular, and the time interval step can be conveniently modified without changing the distance step. It is very significant to decrease the computing time and conduct synchronous iteration for complicated pipe net systems, based on the same concise structure and program as the explicit MOC format.

4.4.2 Meshing of pipes in series

In the traditional model, it is very difficult to mesh a pipe with the same time increment, which is necessary to conduct simultaneous computation. In other words, in meshed pipes, all pipes in the system need to meet the following equations [1]:

$$\Delta t = \frac{l_i}{a_i n_i}. \tag{26}$$

Considering the different wave speeds and pipe lengths, it is very difficult to meet the above condition in most pipe systems, especially a complicated pipe network. In general, it is necessary to adjust the wave speed or the pipe length in order to keep the same time step for all pipes. Sometimes, if a very short pipe is connected in the pipe system, a very small time step is necessary, which will also fix the space steps of other pipes according to Eq. (24). Absolutely, it increases the computational difficulty and the time consumed. Conversely, in the same conditions, MITS can adopt a larger space step for other pipes according to Eq. (26).

In the proposed model, the time step is no longer subjected to the space step according to the characteristic line. Consequently, it is very convenient to use a consistent time step, especially for a complicated pipe network. The proposed method is more convenient in executing simultaneous calculation and saving time. Figure 12a shows the meshing process in MOC, where the indivisible remainder needs to be re-meshed by adjusting the wave speed according to the characteristic line. Obviously, Fig. 12b shows the simpler meshing process in the proposed method without limit of the characteristic line

4.4.3 Sensitivity analysis of time consumed

For a specific wave period, generally, numerous data points are required to capture the peak pressure value and describe the accurate waveform; in other words, the time step should be small enough to describe the entire

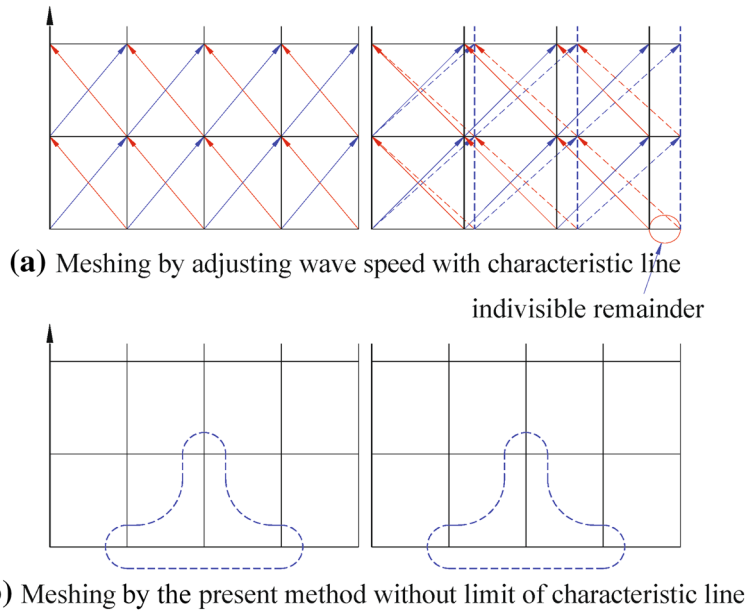

Fig. 12 Comparison of meshing in $x - t$ grid for variable–property pipes in series

Table 1 Dimensionless space step and time consumption

C_R	Δt (s)	C_{xMO}	C_{xMT}	T_{MO} (s)	T_{MT} (s)	C_{TMO}	C_{TMT}	C_{TR}
1	0.1000	1.00*	1.00	0.1289	0.4102	1.00	3.18	3.18
2	0.0500	0.50*	1.00	0.3711	0.8516	2.88	6.61	2.29
3	0.0333	0.33*	1.00	0.7773	1.3203	6.03	10.24	1.70
4	0.0250	0.25*	1.00	1.4023	1.7266	10.88	13.39	1.23
5	0.0200	0.20*	1.00	2.1719	2.1602	16.85	16.76	0.99
6	0.0167	0.17*	1.00	3.0586	2.6094	23.73	20.24	0.85
7	0.0143	0.14*	1.00	4.2305	2.9922	32.82	23.21	0.71
8	0.0125	0.13*	1.00	5.4219	3.4805	42.06	27.00	0.64
9	0.0111	0.11*	1.00	6.9180	3.8516	53.67	29.88	0.56
10	0.0100	0.10*	1.00	8.4883	4.3008	65.85	33.36	0.51

waveform accurately. The comparison in Fig. 6 shows that the proposed method can accurately predict the water hammer waveform. In order to analyze the influence of meshing on the time consumed, we have chosen a basic MOC grid as the reference, the time step as $\Delta t_0 = 0.1$ s, and the basic space step as $\Delta x_0 = 10$ m in the first pipe and $\Delta x_0 = 12$ m in the second pipe, $T_0 = 0.1406$ s. Based on the reference, Table 1 shows the dimensionless space step and time consumption, which are defined as $C_R = \Delta t_0/\Delta t$, $C_x = \Delta x/\Delta x_0$, $C_T = T/T_0$, $C_{TR} = T_{MT}/T_{MO}$. As shown in Table 1, when we refined the waveform in MTMS, the space step is not subjected to the change of the time step. However, in MOC, the space step must be simultaneously adjusted with the decrease in the time step according to the characteristic line. In the table, the symbol* denotes that the space step depends on the time step in the MOC model. Accordingly, Fig. 13 shows that the time consumed decreases with the increase in the time interval step. As shown in the figure, MOC will require more time for an accurate waveform, since the space interval step must match the change of time interval step. On the contrary, the proposed method can still use the original space interval step when the time step is refined, so the increase in time consumption is less than in the MOC.

As shown in Fig. 13, when the same time and space interval $x - t$ grid are used, the MTMS takes a little more computing time, since it has an extra estimating process in the MacCormack time marching scheme. However, its space step is not subjected to the constraint of the characteristic line; thus, MTMS can save more time when using an extended space step.

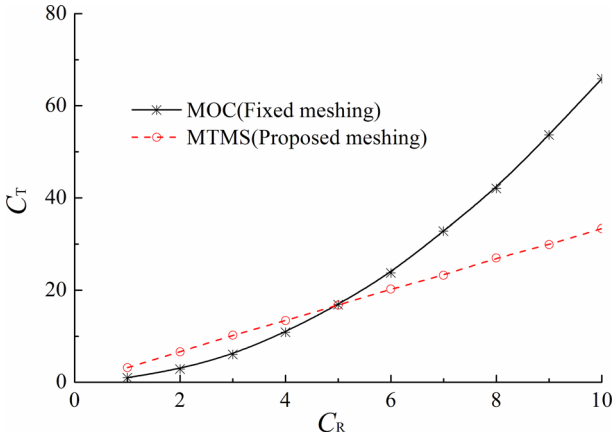

Fig. 13 Time consumed with the density of time step

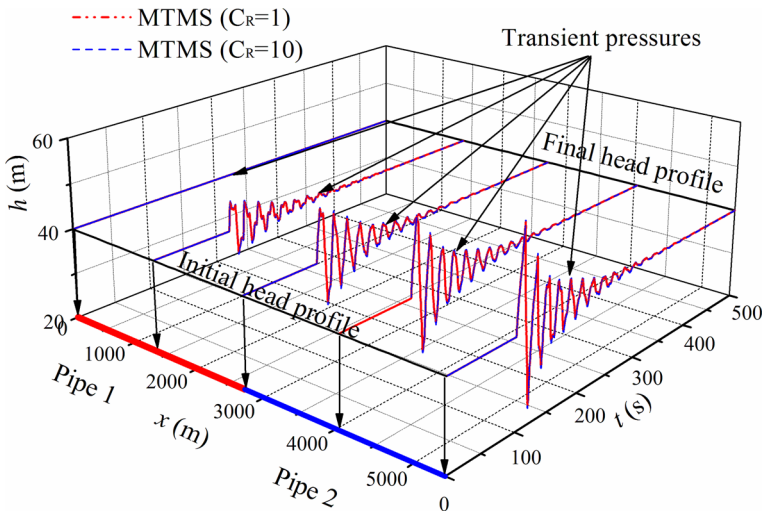

Fig. 14 Comparison of transient pressure process simulated with different time interval steps

4.4.4 Influence of modified time interval on the numerical result in MTMS

In order to analyze the influence of the time steps on the numerical precision, Fig. 14 shows the various numerical solutions with different time interval steps, based on the same space step. The results show that a reasonable adjustment in time step increment has hardly influence on the numerical results of the transient pressures. Consequently, a modified time interval step can be used to decrease the computing time without changing the space step increment.

4.4.5 Saving time by increasing the space interval step

As shown in the above analysis, in MTMS, the time interval step and the space step can be adjusted to a certain extent without change in the numerical precision. Given the time interval step, various space interval steps can also be adjusted to decrease the computing time, since the $x - t$ is no longer subjected to the integral process along the characteristics path line. For a specific time interval, without distorting the water hammer waveform, a larger space step can save time for the computing process. Table 2 shows the time consumed for different space steps for a fixed time interval step. As shown in Fig. 15, the runtime decreases significantly with the increase in the space interval step. Figure 16 shows that the increase in the space interval step hardly affects the numerical results of water hammer in a closed pipe. Consequently, without changing the time step, the computing time decreases by adopting a larger space interval (length of element).

Table 2 Sensitivity of time consumed with the refining mesh

C_x	Δt (s)	T_{MT} (s)	C_{TMT}
1	0.01	7.613	1.000
2	0.01	3.828	0.503
3	0.01	2.551	0.335
4	0.01	1.910	0.251
5	0.01	1.520	0.200
6	0.01	1.270	0.167
7	0.01	1.109	0.146
8	0.01	0.961	0.126
9	0.01	0.859	0.113
10	0.01	0.781	0.103

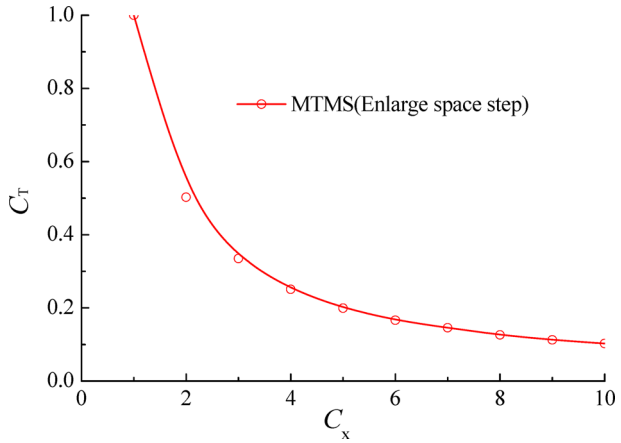

Fig. 15 Sensitivity analysis of the space interval steps on time consumed

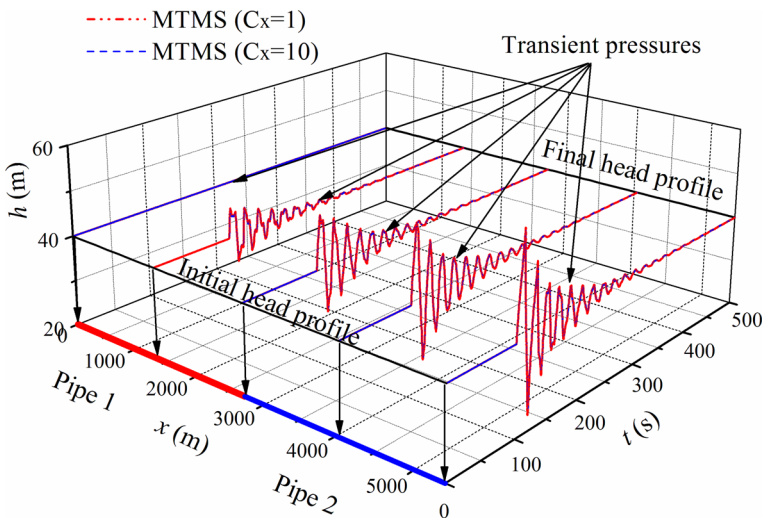

Fig. 16 Comparison of transient pressure process simulated with different space interval steps

5 Analysis and discussion

Compared with MOC, the proposed approach can directly solve the partial differential equation without omitting the convective acceleration term. In theory, the proposed approach includes the pipe flow velocity's influence on the transient wave propagation, and it is important for water hammer simulations with higher flow velocity and low wave speed. It is more convenient without the specified path dependence for the integral of the

partial difference equations in MOC when establishing the $x - t$ time marching mesh. In MOC, it is difficult to establish a uniform $x - t$ time marching mesh for a variable–property series pipe system. However, the approach can more conveniently compute the hydraulic transient in variable–property pipes in series, because a uniform time step can be established by modifying the space steps for serial pipes without the constraint of the characteristic line. Consequently, it is simpler to implement a simultaneous solution process using the MTMS time marching scheme, considering the desired time and space steps for a series pipe system. Moreover, the proposed approach is simpler in dealing with the valve boundary condition than the MOC method. A regular $x - t$ grid mesh is always available, even if the wave propagation is considered as the coupling of water hammer speed and flow velocity. Obviously, the MTMS is still as concise in structure and process as MOC. Though an estimation process is needed in the iteration, it is better simplified without the integral process and limitation of the characteristic line in MOC. In summary, MTMS has the following advantages: (i) MTMS takes less time than MOC when refining the time interval step to obtain an accurate waveform. In other words, a smaller time step can be used for a specified space step. (ii) It can simplify the simultaneous calculation for variable–property pipes, since the identical time interval steps are available for different space steps in the $x - t$ grid. (iii) Boundary conditions, especially valve boundary condition, can be considerably simplified. (iv) The proposed model couples the influence of flow velocity on the wave propagation. (v) The time step and space step can be set up as desired within the Courant condition.

6 Conclusions

An alternative water hammer numerical model is established by using the MacCormack time marching scheme. The boundary conditions are also established with more simplified and distinct processes. The result of simulation with MTMS agreed well with that of MOC. It shows that the proposed method can yield a reasonable numerical solution for the equations in water hammer simulation. Since the MTMS considers the convective acceleration term, which is usually omitted to simplify the water hammer equations in traditional numerical simulations, it is better suited for various water hammer simulations. The regular mesh is still available in the MTMS, so it simplifies the numerical scheme and simultaneous solving process for variable–property pipes in series, since it is not subjected to integration along the specific characteristic line. Moreover, the proposed approach can save computing time by modifying the space step increment.

Acknowledgements We would like to thank Mr. Anton Bergant for supporting our works by sharing his research studies with us.

References

1. Wylie, E.B., Streeter, V.L., Suo, L.: Fluid Transients in Systems. Prentice Hall, Englewood Cliffs (1993)
2. Triki, A.: Water-hammer control in pressurized-pipe flow using an in-line polymeric short-section. Acta Mech. **227**(3), 777–793 (2016). https://doi.org/10.1007/s00707-015-1493-1
3. Triki, A.: Dual-technique-based inline design strategy for water-hammer control in pressurized pipe flow. Acta Mech. (2017). https://doi.org/10.1007/s00707-017-2085-z
4. Rezghi, A., Riasi, A.: Sensitivity analysis of transient flow of two parallel pump-turbines operating at runaway. Renew. Energy **86**, 611–622 (2016). https://doi.org/10.1016/j.renene.2015.08.059
5. Li, X., Zhu, M., Xie, J.: Numerical simulation of transient pressure control in a pumped water supply system using an improved bypass pipe. Strojniski Vestn. J. Mech. Eng. **62**(10), 614–622 (2016). https://doi.org/10.5545/sv-jme.2016.3535
6. Rohani, M., Afshar, M.H.: Simulation of transient flow caused by pump failure: point-implicit method of characteristics. Ann. Nucl. Energy **37**(12), 1742–1750 (2010). https://doi.org/10.1016/j.anucene.2010.07.004
7. Yu, X.D., Zhang, J., Miao, D.: Innovative closure law for pump-turbines and field test verification. J. Hydraul. Eng. (2015). https://doi.org/10.1061/(asce)hy.1943-7900.0000976
8. Riasi, A., Tazraei, P.: Numerical analysis of the hydraulic transient response in the presence of surge tanks and relief valves. Renew. Energy **107**, 138–146 (2017). https://doi.org/10.1016/j.renene.2017.01.046
9. Ghidaoui, M.S., Zhao, M., McInnis, D.A., Axworthy, D.H.: A review of water hammer theory and practice. Appl. Mech. Rev. **58**(1), 49–76 (2005)
10. Ghidaoui, M.S., Karney, B.W.: Equivalent differential-equations in fixed-grid characteristics method. J. Hydraul. Eng. ASCE **120**(10), 1159–1175 (1994). https://doi.org/10.1061/(asce)0733-9429(1994)120:10(1159)
11. Afshar, M.H., Rohani, M.: Water hammer simulation by implicit method of characteristic. Int. J. Press. Vessels Pip. **85**(12), 851–859 (2008). https://doi.org/10.1016/j.ijpvp.2008.08.006
12. Chaudhry, M., Hussaini, M.: Second-order accurate explicit finite-difference schemes for waterhammer analysis. J. Fluids Eng. **107**(4), 523–529 (1985)

13. Guinot, V.: Riemann solvers for water hammer simulations by Godunov method. Int. J. Numer. Methods Eng. **49**(7), 851–870 (2000). https://doi.org/10.1002/1097-0207(20001110)49:7<851::aid-nme978>3.0.co;2-#
14. Wood, D.J.: Waterhammer analysis—essential and easy (and efficient). J. Environ. Eng. ASCE **131**(8), 1123–1131 (2005). https://doi.org/10.1061/(asce)0733-9372(2005)131:8(1123)
15. Kim, S.H.: Impulse response method for pipeline systems equipped with water hammer protection devices. J. Hydraul. Eng. ASCE **134**(7), 961–969 (2008). https://doi.org/10.1061/(asce)0733-9429(2008)134:7(961)
16. Kim, S.H.: Dynamic memory computation of impedance matrix method. J. Hydraul. Eng. ASCE **137**(1), 122–128 (2011). https://doi.org/10.1061/(asce)hy.1943-7900.0000278
17. Niroomandi, A., Borghei, S.M., Bohluly, A.: Implementation of time splitting projection method in water hammer modeling in deformable pipes. Int. J. Press. Vessels Pip. **98**, 30–42 (2012). https://doi.org/10.1016/j.ijpvp.2012.07.002
18. Alamian, R., Behbahani-Nejad, M., Ghanbarzadeh, A.: A state space model for transient flow simulation in natural gas pipelines. J. Nat. Gas Sci. Eng. **9**, 51–59 (2012). https://doi.org/10.1016/j.jngse.2012.05.013
19. Hwang, Y.H.: Development of a characteristic particle method for water hammer simulation. J. Hydraul. Eng. **139**(11), 1175–1192 (2013). https://doi.org/10.1061/(asce)hy.1943-7900.0000771
20. Bazargan-Lari, M.R., Kerachian, R., Afshar, H., Bashi-Azghadi, S.N.: Developing an optimal valve closing rule curve for real-time pressure control in pipes. J. Mech. Sci. Technol. **27**(1), 215–225 (2013). https://doi.org/10.1007/s12206-012-1208-7
21. Karadzic, U., Bulatovic, V., Bergant, A.: Valve-induced water hammer and column separation in a pipeline apparatus. Strojniski Vestn. J. Mech. Eng. **60**(11), 742–754 (2014). https://doi.org/10.5545/sv-jme.2014.1882
22. Holler, S., Jaberg, H.: A contribution to water hammer analysis in pumped-storage power plants. Wasserwirtschaft **103**(1–2), 78–84 (2013)
23. Wan, W., Li, F.: Sensitivity analysis of operational time differences for a pump-valve system on a water hammer response. J. Press. Vessel Technol. **138**(1), 011303 (2016). https://doi.org/10.1115/1.4031202
24. Vasconcelos, J.G., Klaver, P.R., Lautenbach, D.J.: Flow regime transition simulation incorporating entrapped air pocket effects. Urban Water J. **12**(6), 488–501 (2015). https://doi.org/10.1080/1573062x.2014.881892
25. Travas, V., Basara, S.: A mixed MOC/FDM numerical formulation for hydraulic transients. Tech. Gaz. **22**(5), 1141–1147 (2015)
26. MacCormack, R.: The effect of viscosity in hypervelocity impact cratering. J. Spacecr. Rockets **40**(5), 757–763 (2003)
27. Gottlieb, D., Turkel, E.: Dissipative two–four methods for time-dependent problems. Math. Comput. **30**(136), 703–723 (1976). https://doi.org/10.2307/2005392
28. Anderson, J.D.: Computational Fluid Dynamics: The Basics with Applications. McGrawhill Inc, New York (1995)
29. Triki, A.: Resonance of free-surface waves provoked by floodgate maneuvers. J. Hydrol. Eng. **19**(6), 1124–1130 (2014). https://doi.org/10.1061/(asce)he.1943-5584.0000895
30. Triki, A.: Further investigation on the resonance of free-surface waves provoked by floodgate maneuvers: negative surge waves. Ocean Eng. **133**, 133–141 (2017). https://doi.org/10.1016/j.oceaneng.2017.02.003
31. Amara, L., Berreksi, A., Achour, B.: Adapted MacCormack finite-differences scheme for water hammer simulation. J. Civ. Eng. Sci. **2**(4), 226–233 (2013)
32. Bergant, A., Simpson, A.R.: Estimating unsteady friction in transient cavitating pipe flow. In: 2nd International Conference on Water Pipeline Systems, Edinburgh, Scotland (1994)
33. Bergant, A., Vitkovsky, J., Simpson, A.R., Lambert, M.: Valve induced transients influenced by unsteady pipe flow friction. In: 10th International Meeting of the Work Group on the Behaviour of Hydraulic Machinery under Steady Oscillatory Conditions, pp. 12–23 (2001)
34. Bergant, A., Simpson, A.R., Vitkovsky, J.: Developments in unsteady pipe flow friction modelling. J. Hydraul. Res. **39**(3), 249–257 (2001). https://doi.org/10.1080/00221680109499828
35. Zielke, W.: Frequency-dependent friction in transient pipe flow. J. Basic Eng. **90**(1), 109–115 (1968)
36. Hino, M., Sawamoto, M., Takasu, S.: Study on the transition to turbulence and frictional coefficient in an oscillatory pipe flow. Trans. JSCE **9**, 282–284 (1977)
37. Brunone, B., Golia, U.M., Greco, M.: Some remarks on the momentum equation for fast transients. In: Proceedings of International Conference on Hydraulic Transients With Water Column Separation, pp. 201–209 (1991)
38. Pezzinga, G.: Discussion of 'Developments in unsteady pipe flow friction modelling'. J. Hydraul. Res. **40**(5), 650–653 (2002)
39. Pezzinga, G.: Evaluation of unsteady flow resistances by quasi-2D or 1D models. J. Hydraul. Eng. ASCE **126**(10), 778–785 (2000). https://doi.org/10.1061/(asce)0733-9429(2000)126:10(778)
40. Vardy, A.E., Brown, J.M.B.: Transient turbulent friction in smooth pipe flows. J. Sound Vib. **259**(5), 1011–1036 (2003). https://doi.org/10.1006/jsvi.2002.5160
41. Brunone, B., Ferrante, M., Calabresi, F.: Discussion of "Evaluation of unsteady flow Resistances by Quasi-2D or 1D models" by Giuseppe Pezzinga. J. Hydraul. Eng. ASCE **128**(6), 646–647 (2002). https://doi.org/10.1061/(asce)0733-9429(2002)128:6(646)
42. Urbanowicz, K., Zarzycki, Z.: Improved lumping friction model for liquid pipe flow. J. Theor. Appl. Mech. **53**(2), 295–305 (2015)
43. Ioriatti, M., Dumbser, M., Iben, U.: A comparison of explicit and semi-implicit finite volume schemes for viscous compressible flows in elastic pipes in fast transient regime. ZAMM-Zeitschrift Für Angewandte Mathematik und Mechanik **97**(11), 1358–1380 (2017). https://doi.org/10.1002/zamm.201700018
44. Ioriatti, M., Dumbser, M.: Semi-implicit staggered discontinuous Galerkin schemes for axially symmetric viscous compressible flows in elastic tubes. Comput. Fluids **167**, 166–179 (2018). https://doi.org/10.1016/j.compfluid.2018.02.019
45. Vardy, A.E., Brown, J.M.B.: On turbulent, unsteady, smooth-pipe flow. In: International Conference on Pressure Surges and Fluid Transients, Harrogate, England, pp. 289–311. BHR Group (1996)